JTTEE5 16:498–505
DOI: 10.1007/s11666-007-9068-x
1059-9630/$19.00 © ASM International

Peer Reviewed

Low Thermal Conductivity Coatings for Gas Turbine Applications

N. Markocsan, P. Nylén, J. Wigren, and X.-H. Li

(Submitted October 11, 2006; in revised form April 24, 2007)

Plasma spraying of thermal barrier coatings (TBCs) on gas turbine parts is widely used today either to enable higher-turbine inlet temperatures with consequent improvement of combustion efficiency or to reduce the requirements for the cooling system and increase component life-time. Development of low conductivity TBCs, which allows us to further increase gas turbine efficiency and availability, is an ongoing challenge. In order to get low thermal conductivity values an experimental program was conducted. Yttria partially stabilized zirconia (YPSZ) and dysprosia partially stabilized zirconia (DyPSZ) were used to study the influence of power input in the plasma torch and powder feed rate on coating properties. Microstructure evaluations were performed to evaluate the influence of the spraying parameters on the coating morphology and porosity level. Laser Flash (LF) and Transient Plane Source (TPS) methods were utilized to evaluate the coatings thermal conductivity and a comparison between the two methods conducted as well as a correlation study between coating microstructure/composition and thermal conductivity (TC).

Keywords plasma spray, TBCs, porosity, thermal conductivity, zirconia

1. Introduction

A key factor in improving gas turbine engine power and fuel efficiency is the gas operating temperature. Many efforts have been devoted in the past decades to reach higher combustion temperatures (Ref 1, 2). Higher combustion temperatures demands either enhanced cooling efficiency or improved thermal resistance in combustion chamber walls. The potential to further develop Ni-based superalloys seems limited. The maximum temperature is close to 1000 °C where the material looses strength and oxidation resistance (Ref 3). Reduction of the in service part temperature is therefore usually accomplished by the use of thermal barrier coatings. The selection of TBC materials is restricted by some requirements: (1) high melting point, (2) no phase transformation between room temperature and operation temperature, (3) low thermal conductivity, (4) chemical inertness, (5) low thermal expansion mismatch with the metallic substrate, (6) good adherence to the metallic substrate, and (7) low sintering rate of the porous microstructure (Ref 4). Not many materials have been found to satisfy these requirements and continuous research is performed to find new materials. Zirconia (ZrO_2) is an attractive TBC material due to its low thermal conductivity and, compared to other ceramics, has superior mechanical properties, such as high strength and fracture toughness combined with good wear resistance and, above all, a thermal expansion coefficient close to that of metallic substrates (Ref 5, 6).

Zirconia exists in three crystallographic phases: the low-temperature monoclinic phase; the intermediate-temperature tetragonal phase; and the high-temperature cubic phase. As temperature is changed the phase transformation of tetragonal to monoclinic phase is accompanied by significant volume expansion (approximately 3-5 vol%) which induces stresses and failure of the TBC system. Addition of oxides can stabilize the high-temperature cubic phase in zirconia, so the occurrence of monoclinic zirconia can be repressed. The main stabilizers used widely in TBC applications are: Y_2O_3, CeO_2, MgO, and CaO added in different amounts to zirconia powders. The good mechanical properties and stability combined with low thermal conductivity of plasma sprayed partially-stabilized zirconia with yttria (7-8 wt%), have led to its widest use as TBC material in industrial applications (Ref 7, 8). Other studies have demonstrated that partial (or total) substitution of Y and/or Zr ions with different mass ions (mainly rare-earth metals) can decrease the thermal conductivity (Ref 9, 10). The addition of oxides of some rare-earth metals such as: dysprosium, cerium, lanthanum, and ytterbium contribute to lower thermal conductivity and higher thermal expansion of sprayed coatings and also improve their stability at elevated temperatures (Ref 9, 11).

Coatings morphology also plays an important role on the TBCs characteristics and life-time. Pores and cracks present in the coating provide an additional heat barrier but also provide some degree of compliance to coatings exposed to large thermo-mechanical loadings. Based on

N. Markocsan and **P. Nylén,** Department of Technology, Mathematics and Computer Science, University West, Trollhättan, Sweden; **J. Wigren,** Surface Technology, Volvo Aero Corporation, Trollhättan, Sweden; and **X.-H. Li,** Department of GRDM, Siemens Industrial Turbomachinery, Finspång, Sweden. Contact e-mail: nicolaie.markocsan@hv.se.

geometrical considerations of each void in the microstructure, the total porosity in a coating can broadly be subdivided into pores and cracks. The pores are generally associated to inter and intrasplats globular voids and usually result either from rapid solidification of the lamellae or from incompletely molten particles. Cracks can also be divided in intersplat cracks (delaminations) and intrasplat cracks. Delaminations are mostly parallel to the substrate and are formed between the lamellae during deposition, due to bad contact between lamellae. Intrasplat cracks are mostly vertically oriented and are associated with thermal stress relief. The effectiveness of porosity as thermal barrier depends mainly on: pores and cracks ratio, cracks orientation, voids distribution as well as coating density (Ref 9, 12, 13).

The aim of this study was to develop TBC coatings with low thermal conductivity, able to work at elevated temperatures. The influence of powder chemistry and coating porosity on TBC thermal conductivity was of specific interest. Two thermal conductivity measurement techniques were utilized for comparative purposes.

2. Experimental Methods and Materials

2.1 Materials and Specimen Preparation

The spraying experiments were carried out by atmospheric plasma spraying (APS) using a Sulzer Metco-F4 plasma gun and a combination of Ar/H_2 as plasma gas. The coatings were deposited onto specimens of a grit-blasted Nickel based alloy (Hastelloy X) with two different geometries: square plates ($25 \times 25 \times 1.5$ mm) and round coupons ($\phi 25 \times 5$ mm). In order to spray the ceramic top coat, 300-450 μm in thickness, three zirconia based powders were used as shown in Table 1.

The influence of power input in the plasma torch and powder feed rate on coating properties was analyzed. Previous work (Ref 9), utilizing Design of Experiments, has shown that these two parameters are among the most important factors controlling thermal conductivity. All other parameters were kept as follows: arc current 600 ± 50 A, spray distance 125 ± 25 mm, plasma gas flow rate 45 ± 10 lpm (argon and hydrogen were adjusted to reach the desired power level) and carrier gas 3.0 ± 0.1 lpm. The substrate temperature was <100 °C during sample production. The powder was externally injected using standard powder injectors.

Table 1 Feedstock characteristics of the zirconia powders

Symbol/Manufacturer	Composition	Powder morphology	Particle size, μm
7YPSZ/H.C. Starck	ZrO_2-7 wt% Y_2O_3	A&S*	−90 + 20
8YPSZ/Sulzer Metco	ZrO_2-8 wt% Y_2O_3	HOSP**	−75 + 20
4DyPSZ/Sulzer Metco	ZrO_2-4 mol% Dy_2O_3	HOSP**	−90 + 20

* Agglomerated and sintered
** Homogenized Oven Spheroidized Particles

As listed in Table 2, three spraying regimes were evaluated: SR1—high power and medium feed rate, SR2—high power and high feed rate and SR3—low power and low feed rate. The 100-150 μm thick bondcoat was sprayed using a Ni-based alloy powder (Ni-23Co-17Cr-12Al-0.5Y, in wt.%) with $-75 + 30$ μm particle size.

In order to evaluate the influence of process reproducibility on coating properties, a second set of samples were sprayed using the same operating parameters after a period of 10 months. Agglomerated and sintered 7YPSZ powder was deposited using spraying regime SR1 (A&S 7YPSZ SR1-a and A&S 7YPSZ SR1-b) and "HOSP" 8YPSZ powder was deposited using spraying regime SR3 (HOSP 8YPSZ SR3-a and HOSP 8YPSZ SR3-b).

Prior to thermal conductivity determination, heat treatment was performed using the temperature-time schedule given in Fig. 1. The heat treatment was performed in oven under normal atmospheric conditions. Substrate oxidation during heat treatment was not judged to affect the investigations. The reason for the heat-treatment was to stabilize the ceramic coatings (minimize the microstructure evolution with temperature) as well as to observe the porosity evolution in coatings after heat treatment.

Microstructure evaluations on coatings polished cross-section were carried out using optical microscopy (OM) and scanning electron microscopy (SEM). An image analysis procedure was employed (called Routine IA) which was previously developed within a Brite Euram Project (Ref 9). For further information of this procedure see (Ref 14). By tresholding the grayscale images binary images were produced and the total porosity determined. The total porosity was then separated into closed pores

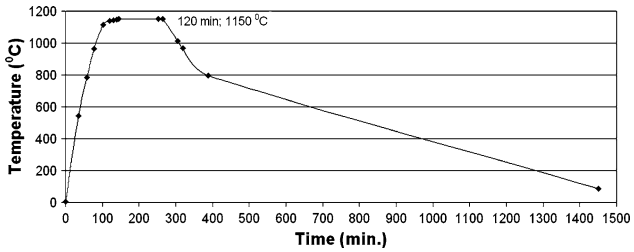

Fig. 1 Diagram of the stabilizing heat treatment

Table 2 Operating parameters

Coating	Powder	Arc power, kW	Powder feed rate, g/min	Spraying regime
A&S 7YPSZ SR1-a	A&S	44.8	90	SR1
A&S 7YPSZ SR2	7YPSZ	44.8	180	SR2
A&S 7YPSZ SR3		38.5	40	SR3
A&S 7YPSZ SR1-b*		44.8	90	SR1
HOSP 8YPSZ SR3-a	HOSP	38.5	40	SR3
HOSP 8YPSZ SR3-b*	8YPSZ	38.5	40	SR3
HOSP 4DyPSZ SR1	HOSP	44.8	90	SR1
HOSP 4DyPSZ SR2	4DyPSZ	44.8	180	SR2
HOSP 4DyPSZ SR3		38.5	40	SR3

*Process reproducibility test samples

(globular voids) and open pores (vertical microcraks and delaminations) through 'dilation' and 'erosion' image analysis operations performed on the binary images, and exploiting the size and shape differences between the globular pores and the crack network. Thus, the distinguishing factor was the area/perimeter ratio (circularity) of each analyzed feature; it was considered a crack if circularity was between 0 and 0.8 respective a globular pore if circularity was greater than or equal to 0.8 and less than or equal to 1. Analysis was performed on 25 distinct areas of the cross-section of each sample. The area covered by each OM micrograph was 429×343 μm. The standard deviation of the employed image analysis method was 0.3%.

2.2 Thermal Conductivity Measurements

2.2.1 Laser Flash (LF). LF is one of the most commonly used methods for measurement of thermal conductivity of coatings. In the laser flash technique (Fig. 2) the front face of a disk shaped specimen is irradiated with a short high-powered laser pulse. The resulting temperature variation of the rear face is then monitored, and thermal diffusivity is calculated from the temperature rise versus time plot.

A disk-shaped free-standing ceramic sample, with a diameter of 10 mm and thickness 300-450 μm, was used for all tests. Thermal diffusivity of the coatings was measured by the finite pulse duration technique (Ref 15) using UMIST equipment (Ref 16). Each sample was coated with a thin layer of carbon before the thermal diffusivity measurement was carried out to prevent reflection of the laser pulse. The samples were tested in argon at or slightly above atmospheric pressure. The heat pulse was supplied by a solid state Nd-glass laser ($\lambda = 1.067$ μm) with a beam diameter of 16 mm. The energy output was in the range 5-95 J, and the pulse dissipation time 0.6 ms. The pulse profile was determined and the finite pulse time effects were corrected using the method developed by Clark and Taylor (Ref 17). The temperature rise of the opposite face was monitored by an In-Sb infrared detector, sensitive to 5.5 μm and having a response time of 1.5 μs. The heat losses were corrected using the method developed by Cowan (Ref 18). Measurements were taken from room temperature to 1000 °C, generally at intervals of every 100 °C. At least 10 measurements were recorded at each temperature interval, and an average calculated.

The thermal conductivity was calculated using the equation:

$$k = \alpha C_p \rho \quad \text{(Eq 1)}$$

where k is the thermal conductivity, α is the thermal diffusivity, C_p is the specific heat, and ρ is the density of the measured material. The C_p values for each measurement temperature were determined by calculation for YPSZ (Ref 19, 20) and by differential scanning calorimetry for DyPSZ from previous work (Ref 9, 21). Average density values were determined using the Archimedes method to 5.0576 g/cm^3 for YPSZ, and to 5.12 g/cm^3 for DyPSZ respectively.

2.2.2 The Transient Plane Source (TPS). TPS technique is a relative recently applied method for thermal transport studies of solid materials which is presented in detail in (Ref 22, 23). The method is based on a procedure by which a single current pulse is applied to a double spiral (TPS) sensor that acts both as heat source and temperature sensor. The TPS sensor is placed—in close contact—between two identical samples to be tested. During the transient pulse the voltage drop over the spiral is monitored. This voltage is directly proportional to the temperature increase of the sensor. From the temperature versus time plot, the thermal conductivity of the sample is calculated (Fig. 3).

The main difference versus the classical hot strip transient method is that the TPS sensor can be regarded as

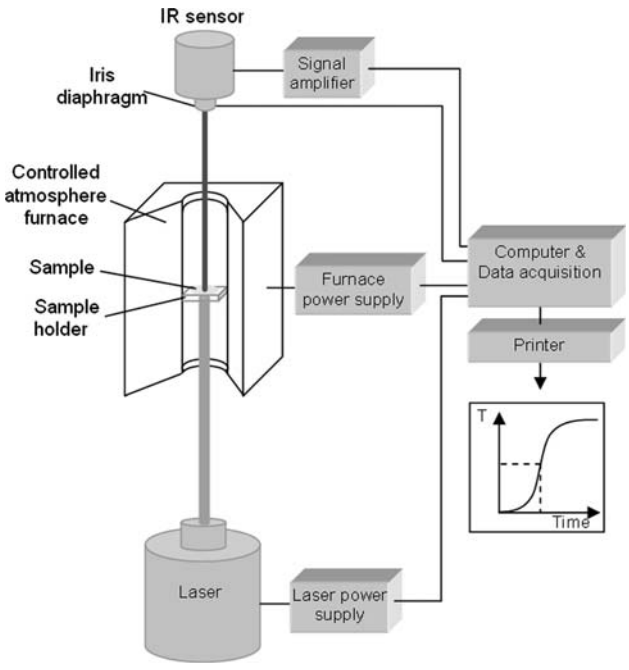

Fig. 2 Schematic of Laser Flash method

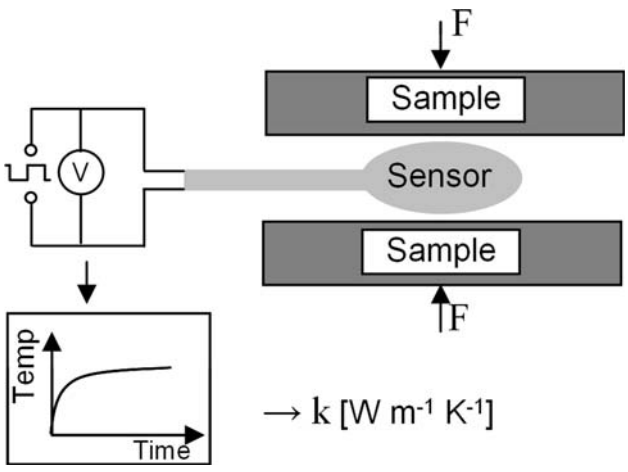

Fig. 3 Schematic of Transient Plane Source technique

a strip wound into a number of concentric circles (in practice a double spiral), then insulated on both sides by a thin polymer with good chemical resistance and mechanical properties. Differently from the hot strip, the TPS sensor is placed between two pieces of the sample material, so all influence on the warming of the sensor during the measurement comes from the sample on both sides. The TPS technique compared to the LF method has shown to be a quicker and cheaper alternative as well as capable to give information about the topcoats' thermal conductivity while it is bonded to substrate.

Round shaped samples 25 mm in diameter were used for these measurements. A disk-shaped sensor with radius of 9.908 mm was used. The employed sensor consists of a double spiral made of nickel foil with thickness of 10 μm covered on both sides with 25 μm thick Kapton layers. The power was 1.0 W and the pulse time was 10 s. For each sample, 4-5 repeated measurements were made, with a resting time of 15 min in-between. The measurements were performed under normal atmospheric and pressure conditions and without removing the ceramic coatings from the substrates. The thermal conductivity measurement of the two layer system samples (bondcoat/topcoat) was performed as follows:

- A preliminary calibration of the sensor was performed to determine the contact resistance induced by the Kapton layer. The sensor was placed between the back sides of the two uncoated substrate samples. The thermal conductivity of the Kapton layer and adhesive toward the sensing spiral were determined;
- Second the thermal conductivity of the bond layer was determined by placing the sensor between two samples coated just with a bondcoat;
- Third a measurement was done on samples coated with both bondcoat and topcoat. The measured thermal conductivity is then an effective thermal conductivity over the two layers (k_{eff}).

The thermal conductivity of the topcoat was finally calculated using Eq. 2.

$$\frac{\sum d_i}{k_{eff}} = \sum \frac{d_i}{k_i} \qquad \text{(Eq 2)}$$

where d_i and k_i are the thickness and the thermal conductivity of the layer i (i refers either to the bondcoat or topcoat). The contribution to the overall thermal conductivity of the thermal contact resistance at the interfaces was not considered.

3. Results and Discussion

3.1 Microstructure

SEM and OM micrographs of the sprayed coatings are presented in Fig. 4-6.

A predominantly lamellar microstructure was achieved with a rather low content of unmolten or partially molten particles. The analyses of all coating micrographs indicated that the degree of particle melting is more dependent on operating conditions than on powder chemistry or

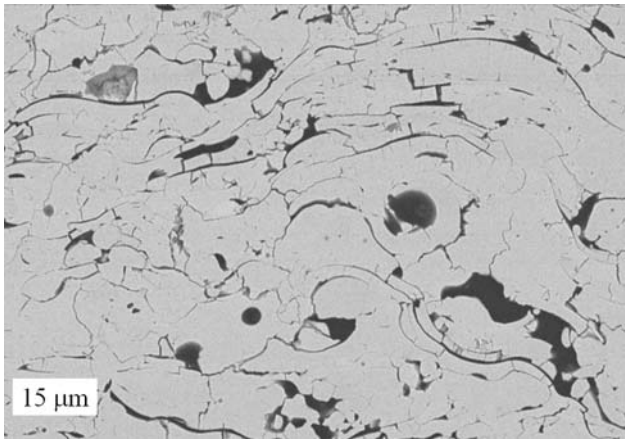

Fig. 4 A&S 7YPSZ SR1, as sprayed, SEM, secondary electron image

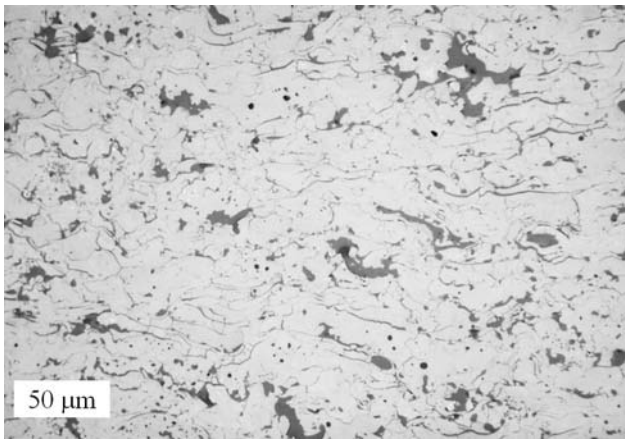

Fig. 5 HOSP 4DyPSZ SR3 after heat treatment, OM

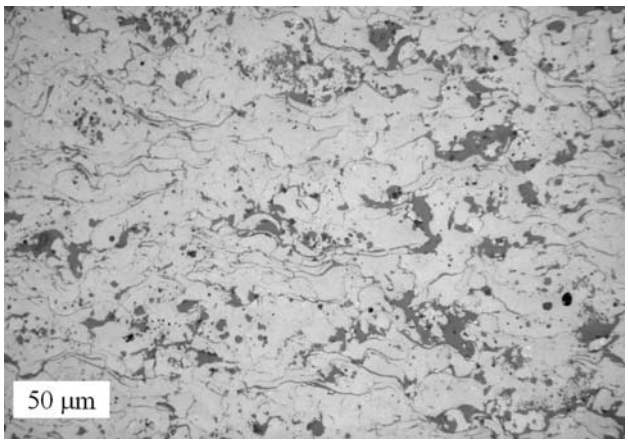

Fig. 6 HOSP 8YPSZ SR3-a, after heat treatment, OM

morphology. Higher energy in the plasma and/or lower powder feed rate led to a better melting of the particles. Both globular voids and cracks were uniformly distributed through the coating cross-sections.

The crack orientations were found to be predominantly parallel to the substrate surface, as can be seen in Fig. 7. The ''HOSP'' powders (both 7YPSZ and 4DyPSZ), due to their morphology, revealed a higher tendency to form delaminations while the agglomerated and sintered (A&S) powders produced cracks with a more arbitrary orientation. Thus more vertical cracks were found within A&S coatings, although their formation was dependent on the spraying conditions, as well.

Figure 8 shows the evolution of the total porosity (in volume percent) of the sprayed coatings, before and after heat treatment and Table 3 shows the individual values of the coating microstructure features. A rather large variation of the total porosity was observed, both for as-sprayed coatings and for heat-treated coatings: 21.3% to 9.2% and 20.3% to 8.2% respectively. In general, the porosity of the coatings decreased after heat treatment. This reduction is attributed to the sintering (fusing) effect acting on small cracks and on small voids. This effect was more pronounced for the ''HOSP'' powders, which showed a higher amount of small-scale porosity and lamellar cracks.

The spraying parameters had an important effect on porosity, the most evident being the formation of big pores. The coatings with the highest porosity were sprayed with low-power input and/or high-powder feed rate. In either of these cases the most significant increase of total porosity was given by the globular pores not by the cracks which seem to be less influenced by the spraying condition (they remain in a relative narrow interval of 4.2-7.2% during all spraying experiments compared to that of voids which is larger 5.0-15.9%).

With regard to the powder chemistry, slightly different behavior was found between spraying YPSZ and DyPSZ powders under the same operating conditions. The total porosity level tended to be lower in DyPSZ coatings than in YPSZ coatings in the case of high plasma energy and significantly decreased when low plasma energy was used and/or with high-powder feed rate. Figure 8 shows that powder morphology was more influential on coating porosity than powder chemistry when high-powder feed rate was used. The coatings sprayed with ''A&S'' powders using spray regime SR2 (A&S 7YPSZ SR2) resulted in almost 10% higher total porosity than the total porosity of the coatings sprayed with ''HOSP'' powders and the same spraying regime (HOPS DyPSZ SR2). The difference between the total porosity of the coatings sprayed with low plasma energy and low-powder feed rate (SR3) was about 4% or less when comparing ''A&S'' with ''HOSP'' coatings and even lower when comparing ''HOSP'' coatings (DyPSZ with YPSZ) i.e., 3.3% between HOSP DyPSZ SR3 and HOSP 8YPSZ SR3-a respectively, 1.8% between HOSP DyPSZ SR3 and HOSP 8YPSZ SR3-b. These latter differences are comparable with those resulted after spraying the HOSP 8YPSZ SR3 in a 10 months interval (−a and −b), thus they are expected not to be due to the coating material itself but rather to the fluctuations in the spray process. Coatings sprayed with high plasma energy (SR1) revealed a significant reduction of the amount of globular voids and no significant difference between their total porosity (Table 3).

Good process reproducibility was achieved, from porosity point of view, with the 7YPSZ powders. A&S 7YPSZ SR1 coatings (−a and −b), sprayed 10 months apart, had almost the same amount of porosity.

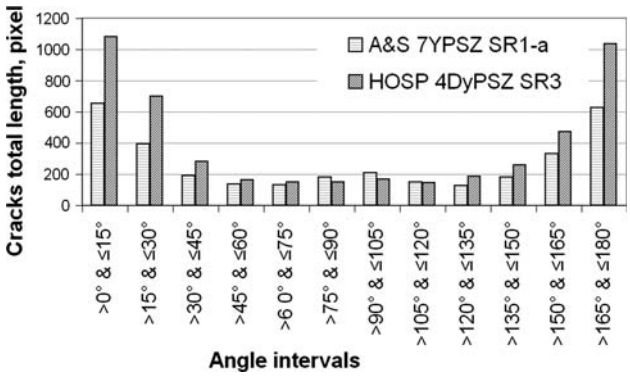

Fig. 7 Crack orientation with respect to substrate surface (0° is parallel to the substrate surface)

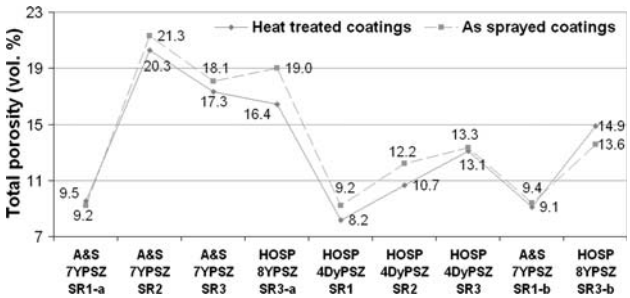

Fig. 8 Evolution of coating total porosity before and after heat treatment

Table 3 Porosity from quantitative image analysis

	Coatings porosity, %			
	As sprayed		After heat treatment	
Coatings	Globular voids	Cracks	Globular voids	Cracks
A&S 7YPSZ SR1-a	5.0	4.2	5.3	4.2
A&S 7YPSZ SR2	15.9	5.4	14.7	5.6
A&S 7YPSZ SR3	12.6	5.5	12.1	5.2
HOSP 8YPSZ SR3-a	11.8	7.2	10.1	6.3
HOSP 4DyPSZ SR1	4.2	5.0	3.8	4.3
HOSP 4DyPSZ SR2	6.7	5.6	5.7	5.0
HOSP 4DyPSZ SR3	7.7	5.6	7.4	5.7
A&S 7YPSZ SR1-b	5.3	4.1	5.2	3.9
HOSP 8YPSZ SR3-b	8.3	5.3	9.0	5.8

3.2 Thermal Conductivity

Figures 9 and 10 present the thermal diffusivity and the thermal conductivity values determined by the Laser Flash

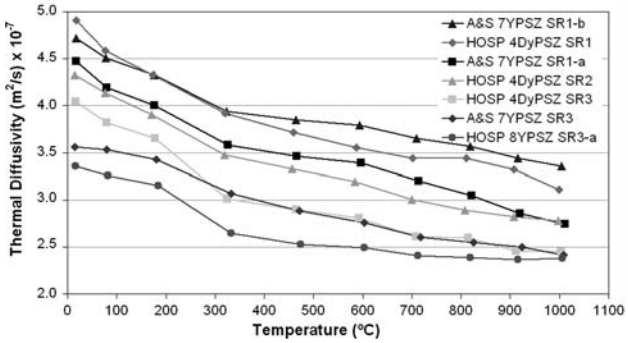

Fig. 9 Measured thermal diffusivity, by LF, 20-1000 °C temperature range

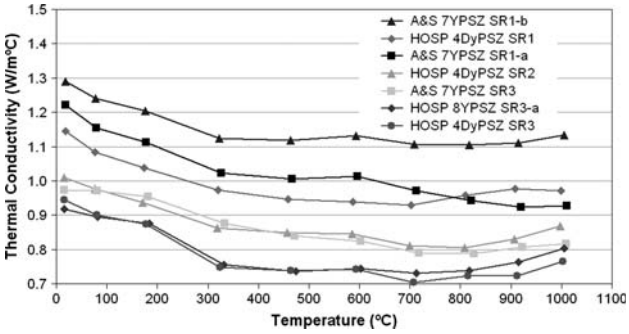

Fig. 10 Calculated thermal conductivity, by LF, 20-1000 °C temperature range

method. All coatings were evaluated except A&S 7YPSZ SR2 and HOSP 8YPSZ SR3-b which were not considered in these measurements.

The results shown in Fig. 9 reveal similar trends in the curves, namely the thermal diffusivity is inversely proportional to temperature. Nevertheless the individual values differ from coating to coating as their microstructure and/or chemistry is changed. Thus the thermal diffusivity of coatings is in the limits of 0.004907-0.003359 cm^2/s at room temperature (RT), and 0.003356-0.002376 cm^2/s at 1000 °C. The descending trend of the thermal conductivity curves, plotted in Fig. 10, indicates a phonon conduction mechanism up to approximately 700-800 °C which is in agreement with previous research (Ref 13, 24–26). At higher temperatures the thermal conductivity (TC) of the majority of the samples increases with temperature which is probably due to the photon conduction mechanism and to the densification of the samples. The latter seems to play a more important role on the coatings' thermal properties at elevated temperatures. Sintering was observed, despite the preheat treatment performed for coating stabilization. The varied ascendant trends of the TC curves above 700 °C (Fig. 10) demonstrate different impacts of the sintering process on the coatings' TC. Coatings with higher density showed a slowly increasing, almost constant or descending TC (A&S 7YPSZ SR1-a), while the TC of porous layers showed a more pronounced ascendance (HOSP 8YPSZ SR3-a).

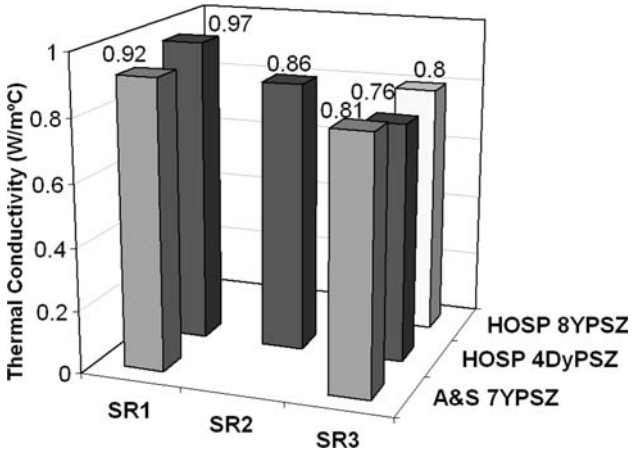

Fig. 11 Influence of the operating conditions and powder composition/morphology on thermal conductivity at 1000 °C

The influence of the operating conditions and powder composition/morphology on the coatings' TC at 1000 °C is presented in Fig. 11.

The coatings' TC dependence on operating conditions was found to correlate well with the porosity of the coatings. Coatings obtained by spraying with high plasma power (low porosity coatings) showed higher TC values while the coatings sprayed with low plasma power or high-powder feed rate (high porosity coatings) showed lower TC values. Powder composition was also found to have an important influence on the coatings' thermal properties. The lowest TC at elevated temperatures (700-1000 °C) was reached with 4DyPSZ powders. The HOSP 4DyPSZ SR3 coating possesses the lowest TC despite its lower porosity (13.1%) compared with 16.4% (HOSP 8YPSZ SR3) and 17.3% (A&S 7YPSZ SR3).

Another factor influencing the coating conductivity is the powder morphology. The HOSP 8YPSZ SR3-a coating revealed the lowest TC at RT among all coatings. Within the whole temperature range (RT-1000 °C) it showed a lower TC than A&S 7YPSZ SR3 which had similar porosity (even higher with 1%) and was sprayed under similar conditions.

Coatings of A&S 7YPSZ SR1 (−a and −b) sprayed with the same operating parameters but at different times in order to observe process reproducibility showed different TC values/variations. This result was surprising because the samples revealed the same porosity. Analyzing the crack orientation, it was found that the first sprayed coating (a) had more horizontal cracks than the later one (b) which possibly acted as thermal insulators, lowering the coating TC. Thus, it has to be due to the reproducibility of the plasma spray processes.

Figure 12 illustrates the room temperature thermal conductivity values for all nine heat-treated zirconia samples, determined by the TPS technique. The corresponding values obtained with LF at 20 °C are also given for comparison. The thermal conductivity values using the TPS technique are in general lower than those obtained with LF (except HOSP 8YPSZ SR3-a coating). The main reason of this discrepancy may come from the

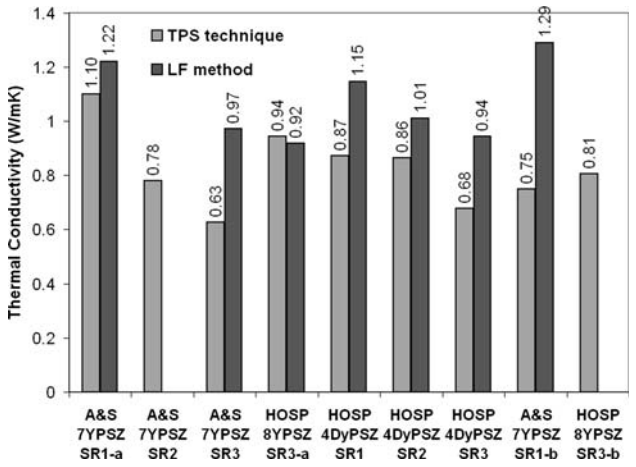

Fig. 12 Thermal conductivity at room temperature measured by TPS and LF

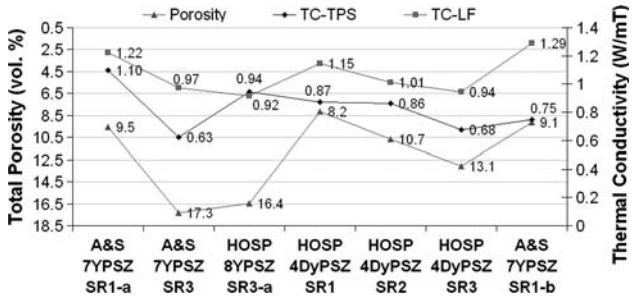

Fig. 13 Plot showing the evolution of thermal conductivity vs. porosity

measurements techniques. The LF measurements were performed on free-standing topcoats while TPS was performed on topcoats bonded to substrates, thus the thermal contact resistance at the interface between topcoat and bondcoat could have affected the TC results obtained with the TPS method. Comparing the TC results obtained by LF and TPS a rather large scatter in the individual TC values from +3% (HOSP 8YPSZ SR3-a) to −72% (A&S 7YPSZ SR1-b) can be observed. This scatter could be attributed to the difficulty in the TPS technique of obtaining good thermal contact to the surface of the tested sample. The measurement accuracy (determined to be in the range of ±5% for both methods) also limits confidence in the results. Further improvement of the TPS technique adapting it to the specific requirements of thermally sprayed coatings could promote it as an interesting alternative method for determination of the thermal properties of coatings.

Figure 13 depicts the evolution of both thermal conductivity curves, at room temperature, as well as the curve of total porosity. The shapes of the curves of thermal conductivity and porosity indicate a good correlation between the thermal transport properties and the microstructural features of the coatings. Better correlation was found between the Laser Flash TC values and porosity. Powder morphology and chemistry are also of importance in controlling the coatings' thermal conductivity although not in a conclusive manner. The exact level of contribution of each factor is yet to be determined.

4. Conclusions

Thermal barrier coatings, using HOSP and A&S powders consisting of 7-8 wt% YPSZ and 4 mol% DyPSZ were produced using atmospheric plasma spraying. Microstructure analyses revealed important relationships between coating morphology and spraying condition, powder morphology and powder composition. Coating thermal properties were significantly influenced by the operating conditions. Good thermal insulation properties were achieved with the HOSP powders having superior capability to form delaminations. The lowest thermal conductivity at high temperatures was reached with the HOSP 4DyPSZ coatings (0.70 W/mK at 700 °C and 0.76 W/mK at 1000 °C), which demonstrated that the powders composition is as influential as coatings porosity or powder morphology.

Determined TC values revealed that the selection of the measurement method is very important. The proper method has to be chosen in accordance to the coatings characteristics as well as to measurements capabilities. An adaptated TPS technique seems as a feasable method for determination of the thermal properties of thermally sprayed coatings.

Process reproducibility is still an impediment in producing coatings with reliable and reproducible properties.

References

1. R.A. Miller, Thermal Barrier Coatings for Aircraft Engines: History and directions, *J. Therm. Spray Technol.*, 1997, **6**(1), p 35-42
2. S.M. Meier and D.K. Gupta, The Evolution of Thermal Barrier Coatings in Gas Turbine Applications, *J. Eng. Gas Turbine Power*, 1994, **116**(1), p 250-257
3. K.S. Ravichandran, K. An, R.E. Dutton, and S.L. Semiatin, Thermal Conductivity of Plasma-Sprayed Monolithic and Multilayer Coatings of Alumina and Yttria-Stabilised Zirconia, *J. Am. Ceram. Soc.*, 1999, **82**(3), p 673-682
4. X.Q. Cao, R. Vassen, and D. Stoever, Ceramic Materials for Thermal Barrier Coatings, *J. Eur. Ceram. Soc.*, 2004, **24**(1), p 1-10
5. C.C. Berndt, Thermal and Mechanical Properties of Thermal Barrier Coatings, *Inter. J. Turbo and Jet Engines*, 1991, **8**(1&2), p 75-82
6. ''Guide to Engineered Materials,'' Adv. Mater. Processes, 158(6), p 159
7. J. Moon, H. Choi, H. Kim, and C. Lee, The Effects of the Heat Treatment on the Phase Transformation Behaviour of Plasma-Sprayed Stabilized ZrO_2 Coatings, *Surf. Coat. Technol.*, 2002, **155**(1), p 1-10
8. M. Tamura, M. Takahashi, J. Ishii, K. Suzuki, M. Sato, and K. Shimomura, Multilayered Thermal Barrier Coating for Land-Based Gas Turbines, *J. Therm. Spray. Technol.*, 1999, **8**(1), p 68-72
9. J. Wigren, High Insulation Thermal Barrier Systems – HITS, Brite Euram Project BE96-3226, 1996
10. D. Zhu, and R.A. Miller, Thermal Conductivity and Sintering Behaviour of Advanced Thermal Barrier Coatings, NASA/TM-2002-211481, Cleveland, OH, March 2002

11. S. Sodeoka, M. Suzuki, T. Inoue, K. Ueno, and S. Oki, Thermal and Mechanical Properties of ZrO_2-CeO_2 Plasma-Sprayed Coatings, *J. Therm. Spray. Technol.*, 1997, **6**(3), p 361-367
12. A. Kulkarni, A. Vaidya, A. Goland, S. Sampath, and H. Herman, Processing Effects on Porosity-Property Correlations in Plasma Sprayed Yttria Stabilised Zirconia Coatings, *Mater. Sci. Eng. A*, 2003, **359**(1/2), p 100-111
13. L. Pawlowski and P. Fauchais, Thermal Transport Properties of Thermally Sprayed Coatings, *Int. Mat. Rev.*, 1992, **37**(6), p 271-289
14. O. Lavigne, Y. Renollet, M. Poulain, C. Rio, P. Moretto, P. Brannvall, and J. Wigren, Microstructural Characterization of Plasma Sprayed Thermal Barrier Coatings by Quantitative Image Analysis, Quantitative Microscopy of High Temperature Materials Conference, Sheffield, UK, 1999
15. W.J. Parker, R.J. Jenkins, C.P. Butler, and G.L. Abort, Flash Method of Determining Thermal Diffusivity, Heat Capacity, and Thermal Conductivity, *J. Appl. Phys.*, 1961, **32**, p 1679-1684
16. R. Taylor, Construction of Apparatus for Heat Pulse Thermal Diffusivity Measurements from 300–3000 K, *J. Phys. E: Sci. Instrum.*, 1980, **13**, p 1193-1199
17. L. M. Clark and R.E. Taylor, Radiation loss in the flash method for thermal diffusivity, *J. Appl. Phys.*, 1975, **46**(2), p 714-719
18. D. Cowan, Pulse method of measuring thermal diffusivity at high temperatures, *J. Appl. Phys.*, 1963, **34**(4), p 926-927
19. R. Brandt, L. Pawlowski, and G. Neuer, Specific Heat and Thermal Conductivity of Plasma Sprayed Yttria-stabilised Zirconia and NiAl, NiCr, NiCrAl, NiCrAlY, NiCoCrAlY Coatings, *High Temp.-High Pressures*, 1986, **18**, p 65-77
20. K.E. Wilkes and J.F. Lagedrost, Thermophysical properties of plasma sprayed coatings, NASA Report NASA-CR-121144, 1973
21. J. Wigren, Improved Plasma Sprayed Thermal Barriers for Relevant Combustor Geometries Using Enhanced Process Control and Better Test Technologies-COMBCOAT, Brite Euram Project BRE-CT94-0936, 1994
22. S. Gustafsson, Transient Plane Source Techniques for Thermal Conductivity and Thermal Diffusivity Measurement of Solid Materials, *Rev. Sci. Instrum.*, 1991, **62**(3), p 797-804
23. T. Log and S.E. Gustafsson, Transient Plane Source (TPS) Technique for Measuring Thermal Transport Properties of Building Materials, *Fire Mater.*, 1995, **19**(1), p 43-49
24. R.E. Taylor, X. Wang, and X. Xu, Thermophysical Properties of Thermal Barrier Coatings, *Surf. Coat. Technol.*, 1999, **120-121**, p 89-95
25. D. Schwingel, R. Taylor, T. Haubold, J. Wigren, and C. Gualco, Mechanical and Thermophysical Properties of Thick PYSZ Thermal Barrier Coatings: Correlation with Microstructure and Spraying Parameters, *Surf. Coat. Technol*, 1998, **108-109**, p 99-106
26. S. Ahmaniemi, P. Vuoristo, T. Mäntylä, F. Cernuschi, and L. Lorenzoni, Modified Thick Thermal Barrier Coatings: Thermophysical Characterization, *J. Eur. Ceram. Soc.*, 2004, **24**, p 2669-2679